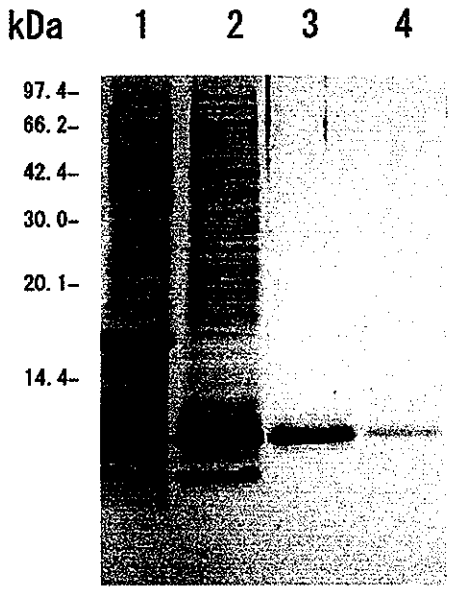

Fig. 4. SDS–PAGE of processed cytochrome b_5 purified from tb5wt. Lane 1, 424,000*g* pellet (38 μg); lane 2, 424,000*g* supernatant (40 μg); lane 3, processed cytochrome b_5 purified from the transformant (after CM-cellulofine column chromatography; 1.42 μg); lane 4, native cytochrome b_5 purified from *A. suum* body wall (0.7 μg). See Materials and methods for details.

freeze–thaw procedure effectively extracted the processed product into the supernatant, whereas the recombinant full-length precursor protein remained in the pellet. Complete purification was achieved in only one ion-exchange chromatography step, appearing in SDS–PAGE as a single band with a mobility the same as that of native cytochrome b_5 purified from *A. suum* body wall (Fig. 4, lanes 3 and 4). The yield of purified protein was 10.6 mg protein per liter of culture.

Molecular mass

The molecular mass of the processed product purified from the transformant was determined by ESI mass spectrophotometry (Fig. 5). Two peaks of 9140.0 and 9755.0 were obtained in deconvolution analysis. The value of 9140.0 is exactly identical to the molecular mass of the apoprotein purified from the nematode body wall, as previously determined [25]. Because the molecular mass of free protoheme is 616.3, the value 9755.0 corresponds to the molecular mass of the holoprotein with the heme. Thus, unlike native cytochrome b_5 [25], processed cytochrome b_5 is not completely denatured under the analysis conditions employed; some portion remains as holoprotein.

Spectral properties

Fig. 6 shows the absorption spectra of the oxidized and dithionite-reduced forms of processed cytochrome

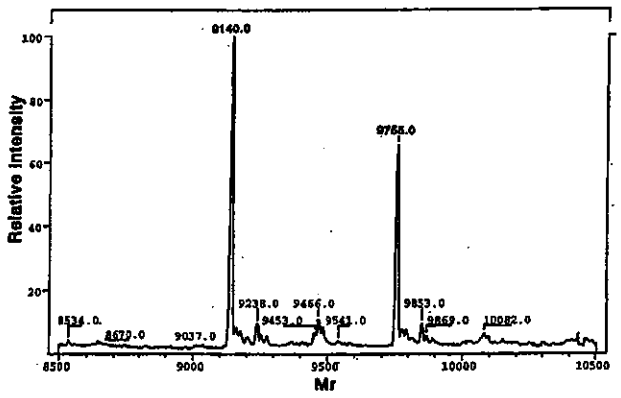

Fig. 5. ESI mass spectrometry of *A. suum*-processed cytochrome b_5 purified from tb5wt. Numerals on the peaks denote deconvoluted values of molecular mass.

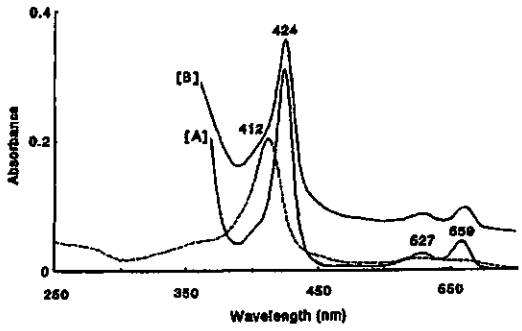

Fig. 6. Absorption spectra of *A. suum*-processed cytochrome b_5 purified from tb5wt and reduction of the cytochrome with NADH in the presence of the nematode microsomal fraction. The processed cytochrome b_5 (1.8 nmol) was diluted with 1 ml of 100 mM Tris–HCl, pH 7.4, in a sample cuvette (1-cm light path), and the absorption spectrum of the oxidized hemoprotein was recorded (dashed trace). Next, a few crystals of sodium dithionite were added to the sample cuvette, and the spectrum of the reduced hemoprotein was recorded after mixing by inversion (trace A). To the sample cuvette containing 1.8 nmol of processed cytochrome b_5 and 0.22 mg of the nematode microsomal fraction in 1 ml of 100 mM Tris–HCl, pH 7.4, 10 μl of 10 mM NADH was added. The solution was mixed by inversion, and left for 2 min, and the spectrum was recorded (trace B).

b_5; absorption bands were observed at 412 nm (γ) in the oxidized form (dashed trace) and at 559 nm (α), 527 nm (β), and 424 nm (γ) in the reduced form (trace A). The spectra are identical to those of native cytochrome b_5 purified from nematode body wall [25]. Furthermore, the extinction coefficients and heme contents of processed and native cytochrome b_5 were determined (Table 2). Coefficient values for processed cytochrome b_5 were comparable to those for native cytochrome b_5. Heme content was higher in processed cytochrome b_5 than in native cytochrome b_5 prepared by several steps of purification; one-step purification of processed cytochrome b_5 likely minimized loss of heme during preparation. A difference extinction coefficient, $\Delta\varepsilon_{red.-oxid}$, was calculated at 424 and 559 nm with values of 107.7 and 14.4 $mM^{-1}\,cm^{-1}$ obtained, respectively.

Table 2
Absorption coefficients and heme contents of native and processed cytochrome b_5[a]

	ε ($mM^{-1}cm^{-1}$)				Heme content (nmol/mg protein)
	Oxidized form	Reduced form			
	412 nm	424 nm	527 nm	559 nm	
Native cytochrome b_5	112.4 ± 7.6	174.6 ± 9.9	11.7 ± 1.9	21.9 ± 1.7	74.9 ± 5.8
Processed cytochrome b_5	107.1 ± 5.5	167.3 ± 9.9	15.0 ± 2.5	24.5 ± 2.0	83.6 ± 5.9

[a] Values are means ± standard deviations of three different determinations.

Reactivity with NADH–cytochrome b_5 reductase

Since cytochrome b_5 functions as an electron carrier between a NAD(P)H–cytochrome b_5 reductase and an acceptor, the reactivity of the processed cytochrome b_5 with the cytochrome b_5 reductase of *A. suum* body wall was studied to estimate its integrity and function. Previous studies on the distribution of NADH–cytochrome b_5 reductase in the subcellular fractions showed its microsomal occurrence with high specific activity (0.28 nmol cytochrome b_5 reduced/min/mg protein). Therefore, whether the processed cytochrome b_5 was reduced with NADH in the presence of the *A. suum* microsomal fraction was examined. As shown in Fig. 6 (trace [B]), the nematode microsomal fraction indeed reduced the cytochrome b_5. The contribution of absorbance derived from microsomal cytochrome *b* [35] reduced with NADH was negligible and no reduction of processed cytochrome b_5 was detected with only NADH (data not shown). Thus, the processed cytochrome b_5 from tb5wt, like native cytochrome b_5, was shown to be reduced by the nematode NADH–cytochrome b_5 reductase.

Discussion

The current data clearly show that the histidine-tagged full-length presequence functions as a signal peptide in *E. coli*; the recombinant precursor protein was accurately processed, as in *A. suum* tissues, and the mature cytochrome b_5, almost chemically and functionally identical to the native protein purified from the nematode, was transported to the periplasm. It is also evident that the full-length presequence plays an important role in this processing function because mutant transformants possessing truncated presequences, tb5Δ18 and tb5Δ28, failed in processing and transporting their recombinant proteins. At present, whether the full-length presequence per se functions as a signal peptide in the bacteria is unknown. However, it should be pointed out that, as shown in Fig. 7, the primary structure of the presequence of *A. suum* cytochrome b_5 appears to fulfill a requirement for a signal, peptide [36]; an amino-terminal, positively charged region (n-region, from the 1st to around the 11th residue in Fig. 7), a central hydrophobic part (h-region, from around the 11th to the 23rd residue), and a more polar carboxy-terminal domain (c-region, from the 24th to the 30th residue), can be assigned in the sequence. Since a positively charged n-region is presumably required for efficient translocation, an additional 9 positively charged amino acid residues in the tag may facilitate binding of the precursor protein to the lipid bilayer of plasma membrane. Alternatively, such a bulk of histidine tag artificially extending from the proper n-region appears not to be a big obstacle, at least, in processing the protein.

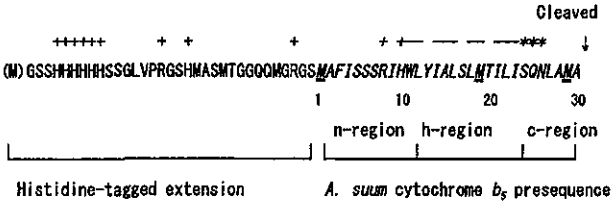

Fig. 7. Primary structure of the histidine-tagged full-length presequence of *A. suum* cytochrome b_5 . The part of the full-length presequence is shown by italic letters with the 1st, 19th, and 29th methionines double-underlined. Positively charged amino acids, such as arginine or histidine, are designated by +. Noncharged polar amino acid residues found in the c-region are asterisked (*). Nonpolar amino acids are marked with –.

It is interesting that significant amounts of recombinant cytochrome b_5 are distributed in the membrane fraction (Table 1). For example, in tb5Δ18, 87.6% of total recoverable cytochrome b_5 was distributed in the membrane fraction as a histidine-tagged recombinant protein as shown in Figs. 3A and B (band *b* in lane 9). Of course, this does not mean that these recombinant proteins are "properly" assembled in the plasma membrane like microsomal cytochrome b_5 because *A. suum* cytochrome b_5 lacks the membrane-anchoring domain at the COOH terminus. Rather, the recombinant cytochrome b_5 may be arrested by insertion of the histidine-tagged truncated presequence into the membrane; truncation of 18 amino acid residues of the proper signal peptide likely resulted in arrest during translocation. Alternatively, it may exist in inclusion bodies coprecipitated with the plasma membranes; the membrane fraction prepared by centrifugation cannot avoid containing inclusion bodies on overexpression of a foreign protein. Interestingly, some processed protein, which

was scarcely observed in tb5Δ28, which lacks a majority of the presequence (Fig. 3B, lane 7), was detected by immunoblotting in the cytoplasmic fraction, but not in the periplasmic fraction, of tb5Δ18 and the recombinant protein (Fig. 3B, bands *b* and *e* in lane 6). Thus, small amounts of the recombinant protein of tb5Δ18 was still cleaved somehow but mislocated in the cytoplasm. In the case of tb5Δ28, less of the recombinant protein (43.4%) was distributed in the membrane fraction (Table 1), indicating that the lack of the majority of the presequence resulted in decreased ability for interaction with the membrane to release the protein into cytoplasm. Thus, the behaviors of the recombinant precursor proteins of *A. suum* cytochrome b_5 and the periplasmic localization of its mature form in *E. coli*, demonstrated in the present study, indicate that the complete presequence is indispensable for both intracellular processing and functional folding of the nematode cytochrome b_5. Further studies on the biosynthesis and localization of this novel type of cytochrome b_5 *in A. suum* are needed. Moreover, the present expression system for the production *of A. suum* cytochrome b_5 provides a simple and rapid means of obtaining this protein, which is chemically and functionally identical to the native protein purified from the nematode tissues as demonstrated here. X-ray crystallographic and functional studies using the processed protein are now in progress in our laboratory.

Acknowledgments

This work was supported in part by a Grant-in-Aid for Scientific Research (C) (Nos. 12670241 and 14570220) from the Ministry of Education, Science, Sports and Culture of Japan. We thank Hiroshi Kasanuki and Emiko Sato for their excellent technical assistance.

References

[1] V. Kostanjevecki, D. Leys, G. Van Driessche, T.E. Meyer, M.A. Cusanovich, U. Fischer, Y. Guisez, J. Van Beeumen, J. Biol. Chem. 274 (1999) 35614–35620.
[2] Y. Yoshida, Y. Tamura-Higashimaki, R. Sato, Arch. Biochem. Biophys. 220 (1983) 467–476.
[3] N. Kouzaki, H. Kawashima, M.C.-M. Chung, S. Shimizu, Biochim. Biophys. Acta 1256 (1995) 319–326.
[4] M.A. Smith, A.K. Stobart, P.R. Shewry, J.A. Napier, Plant Mol. Biol. 25 (1994) 527–537.
[5] C. Bonnerot, A.M. Galle, A. Jolliot, J.-C. Kader, Biochem. J. 226 (1985) 331–334.
[6] R.C. Sanborn, C.M. Williams, J. Gen. Physiol. 33 (1950) 579–588.
[7] T. Yamanaka, S. Tokuyama, K. Okunuki, Biochim. Biophys. Acta 77 (1963) 592–601.
[8] B. Hagihara, N. Sato, T. Yamanaka, in: P.D. Boyer (Ed.), The Enzymes, vol. 11, Oxidation–Reduction, Part A, Academic Press, New York, 1975, pp. 549–593.
[9] R.E. Utecht, D.M. Kurtz Jr., Biochim. Biophys. Acta 953 (1988) 164–178.
[10] G.D. Wheelock, J.G. Scott, Comp. Biochem. Physiol. 101B (1992) 209–215.
[11] V.M. Guzov, H.L. Houston, M.B. Murataliev, F.A. Walker, R. Feyereisen, J. Biol. Chem. 271 (1996) 26637–26645.
[12] T. Yubisui, F. Takahashi, T. Takabayashi, S. Fujiwara, K. Kawamura, J. Biochem. (Tokyo) 129 (2001) 709–716.
[13] C.F. Strittmatter, E.G. Ball, Proc. Natl. Acad. Sci. USA 38 (1952) 19–25.
[14] P. Strittmatter, S.F. Velick, J. Biol. Chem. 221 (1956) 253–264.
[15] P.G. Passon, D.W. Reed, D.E. Hultquist, Biochim. Biophys. Acta 275 (1972) 51–61.
[16] S. Yoshida, T. Yubisui, M. Takeshita, Arch. Biochem. Biophys. 232 (1984) 296–304.
[17] F. Lederer, Biochimie 76 (1994) 674–692.
[18] T. Yubisui, Seikagaku (in Japanese) 66 (1994) 436–442.
[19] G. Vergeres, L. Waskell, Biochimie 77 (1995) 604–620.
[20] J. Mitoma, A. Ito, EMBO J. 11 (1992) 4197–4203.
[21] N. Oshino, T. Omura, Arch. Biochem. Biophys. 157 (1973) 395–404.
[22] S. Kimura, K. Abe, Y. Sugita, FEBS Lett. 169 (1984) 143–146.
[23] S.J. Giordano, A.W. Steggles, Biochim. Biophys. Acta 1172 (1993) 95–100.
[24] D.E. Hultquist, P.G. Passon, Nature (New Biol.) 229 (1971) 252–254.
[25] Y. Yu, H. Yamasaki, K. Kita, S. Takamiya, Arch. Biochem. Biophys. 328 (1996) 165–172.
[26] M. Kozak, J. Biol. Chem. 266 (1991) 19867–19870.
[27] A. Torriani, in: L. Grossman, K. Moldave (Eds.), Methods in Enzymology, vol. 12B, Academic Press, New York, 1968, pp. 212–218.
[28] E. Bernt, H.U. Bergmeyer, in: H.U. Bergmeyer (Ed.), Methods of Enzymatic Analysis, second Engl. Ed., Academic Press, New York, 1974, pp. 624–627.
[29] T.E. King, in: R.W. Estabrook, M.E. Pullman (Eds.), Methods in Enzymology, vol. 10, Academic Press, New York, 1967, pp. 216–222.
[30] N. Sato, B. Hagihara, Cancer Res. 30 (1970) 2061–2068.
[31] S. Takamiya, M.A. Lindorfer, R.A. Capaldi, FEEB Lett. 218 (1987) 277–282.
[32] H. Towbin, T. Staehelin, J. Gordon, Proc. Natl. Acad. Sci. USA 76 (1979) 4350–4354.
[33] E. Antonini, M. Brunori, in: A. Neuberger, E.L. Tatum (Eds.), Hemoglobin and Myoglobin in their Reactions with Ligands, North-Holland Publishers, Amsterdam, 1971, pp. 10–11.
[34] M.A.K. Markwell, S.M. Haas, L.L. Bieber, N.E. Tolbert, Anal. Biochem. 87 (1978) 206–210.
[35] S. Matuda, J. Biochem. (Tokyo) 85 (1979) 343–350.
[36] G. von Heijne, J. Membr. Biol. 115 (1990) 195–201.

Osteopontin Transgenic Mice Fed a High-Cholesterol Diet Develop Early Fatty-Streak Lesions

Kikuo Isoda, MD, PhD; Yashuhiro Kamezawa, MD; Makoto Ayaori, MD; Masatoshi Kusuhara, MD, PhD; Norihiro Tada, PhD; Fumitaka Ohsuzu, MD, PhD

Background—Osteopontin (OPN) is a noncollagenous adhesion protein found at the site of atherosclerotic lesions. However, it has not yet been clarified whether or not OPN can promote atherosclerotic lesions.

Methods and Results We investigated the contribution of OPN to atherosclerosis by evaluating aortic sinus lesions of both OPN transgenic (Tg) and non-Tg mice fed an atherogenic diet (1.25% cholesterol) for 16 weeks. The atherosclerotic lesions were found to be significantly larger in OPN-Tg compared with those in non-Tg (17 859±2010 versus 6469±485 μm^2, $P<0.01$). The lesions in both mice were fatty-streak lesions with an accumulation of mononuclear cells and lipids. We next investigated the production of interleukin (IL)-10 by macrophages from both mice. Compared with the non-Tg mice, a 42% ($P<0.01$) and 73% ($P<0.001$) decrease in the IL-10 production was identified in the OPN-Tg mice either without or with lipopolysaccharide.

Conclusions—The expression of OPN induces fatty-streak lesion formation in mice fed an atherogenic diet and inhibits IL-10 production by macrophages, thus suggesting that OPN plays an important role in the development of fatty-streak lesions in vivo. (***Circulation***. **2003;107:679-681.**)

Key Words: atherosclerosis ■ genes ■ interleukins

Atherosclerosis is initiated by the infiltration of monocytes and T lymphocytes into an activated endothelium, and the expression of osteopontin (OPN) protein was detected in both macrophages and vascular smooth muscle cells (SMCs) within atherosclerotic lesions.[1–4] We recently reported that OPN transgenic (Tg) mice showed an increase in the medial thickness of artery without injury and an increase in the neointimal formation after injury.[5] Taken together, these results suggest that OPN may play an important role in the initial step of atherosclerosis, including the proliferation and migration of smooth muscle cells. However, whether or not OPN can promote atherosclerotic lesions remains to be elucidated. The purpose of the present study was to determine whether OPN has a promoting or inhibitory effect on atherosclerosis in OPN-Tg mice.

Methods

Animals and Diet

Previously characterized OPN-Tg mice[5] bred in our laboratory were used under protocols approved by the National Defense Medical College Board for Studies in Experimental Animals. In the present study, we compared heterozygous OPN-Tg to non-Tg littermates (non-Tg). Beginning at 8 weeks after birth and continuing for 16 weeks, both OPN-Tg and non-Tg mice were fed a high-fat/cholesterol diet containing 15% fat, 1.25% cholesterol, and 0.5% sodium cholate, hereafter referred to as the atherogenic diet. These mice were killed at 24 weeks of age to undergo a plasma lipoprotein analysis and lesion assay.

Plasma Lipid Measurements

On the day of analysis, food was removed from the cages in the morning, and the mice were fasted for 7 hours. The plasma total cholesterol, high-density lipoprotein (HDL) cholesterol, and triglyceride levels were then measured by enzymatic assays as previously described.[6]

Quantification of Aortic Sinus Lesions

The sections containing aortic sinus were prepared as previously reported,[7] with modifications. The area of the lesion was measured with the National Institutes of Health Image 1.55 (public domain software). The values reported represented the mean lesion area from 5 sections for each animal. The extent of atherosclerosis in mouse aorta was also determined with an "en face" method.[8]

Immunohistochemical Studies

Frozen sections were incubated with either a primary rat monoclonal antibody against mouse macrophage, clone MOMA-2 (BioSource International), or a primary goat polyclonal antibody against mouse Interleukin (IL)-10 (Pharmingen). Immunostaining was visualized as previously described.[5]

Analysis of the Ability of IL-10 Production by Macrophages

Resident peritoneal macrophages from both non-Tg and OPN-Tg mice obtained by peritoneal lavage with phosphate-buffered saline

Received November 7, 2002; revision received December 18, 2002;accepted December 19, 2002.

From Internal Medicine I, National Defense Medical College (K.I., Y.K., M.A., M.K., F.O.), Tokorozawa, Japan, and the Division of Biomedical Research Resources, Juntendo University School of Medicine (N.T.), Tokyo, Japan.

Correspondence to Kikuo Isoda, MD, PhD, Internal Medicine I, National Defense Medical College, 3-2, Namiki, Tokorozawa, Saitama, 359-8513, Japan. E-mail isoda@me.ndmc.ac.jp

Circulation is available at http://www.circulationaha.org

DOI: 10.1161/01.CIR.0000055739.13639.D7

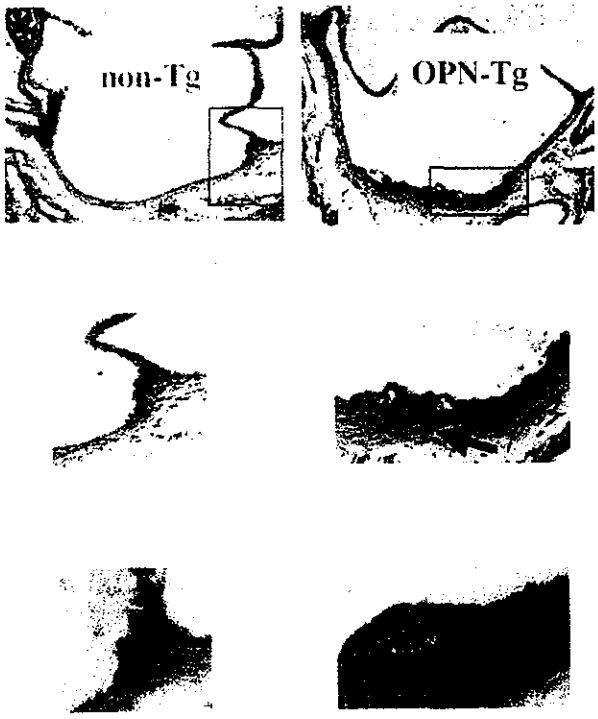

Figure 1. Representative light photomicrographs of aortic atherosclerotic lesions of both non-Tg (left) and OPN-Tg (right). Sections were stained with oil red O and hematoxylin (upper and middle panels). Boxed areas are shown in middle of panels. Arrow shows lipids were contained in the medial layer. The bottom panels show MOMA-2 staining of both mice. Original magnification ×25 (top panels), ×50 (bottom panels), and ×100 (bottom panels).

were treated with red cell lysis buffer and were incubated (10^5 macrophages per 100 μL) for 2 hours. The adherent fraction was incubated with lipopolysaccharide (LPS) (30 ng/mL) for 48 hours. Supernatant IL-10 was assayed with commercial ELISA kits (R&D Systems).

Statistical Analysis

The results are shown as the mean±SE. Two groups were compared with either Student's *t* test or Student-Newman Keuls's test with a one-way analysis of variance. $P<0.05$ was regarded as a significant difference.

Results

Development of Fatty-Streak Lesions

Our previous study demonstrated an increase in the medial thickness of the artery, but no evidence of the formation of early form cells in the OPN-Tg mice fed normal chow.[5] To investigate the impact of OPN on the development of atherosclerotic lesions in vivo, studies were conducted with murine models on an atherogenic diet. After 16 weeks on the atherogenic diet, the total cholesterol (non-Tg: 361.2±15.1 versus OPN-Tg: 325.7±11.3 mg/dL), triglyceride (21.3±2.7 versus 29.2±2.9 mg/dL), and HDL cholesterol levels (58.0±3.8 versus 44.1±3.2 mg/dL), were comparable between the non-Tg (n=12) and OPN-Tg mice (n=12). Figure 1 shows the aortas of both a non-Tg and an OPN-Tg mouse on the atherogenic diet for 16 weeks. There was a marked difference in the lesion size between the OPN-Tg and non-Tg

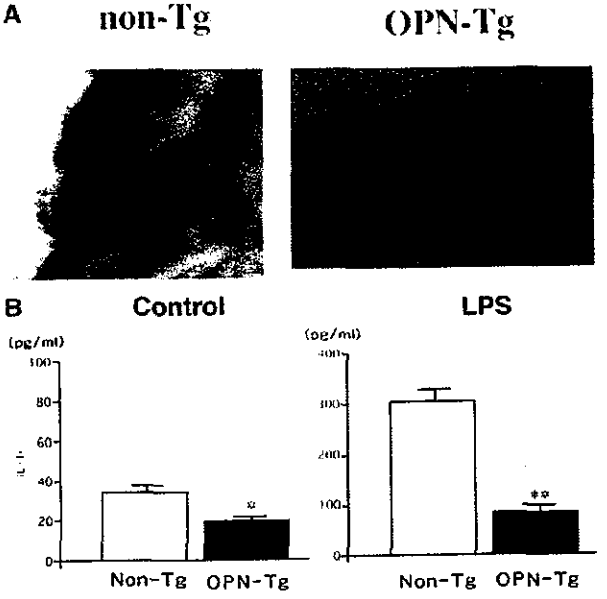

Figure 2. A, Representative photomicrographs showing the immunohistochemical staining for IL-10 in atherosclerotic lesions of non-Tg (left) and OPN-Tg (right). IL-10 expression was detected in the lesion of non-Tg (brown staining). Original magnification ×150. B, Production of IL-10 by peritoneal macrophages from non-Tg and OPN-Tg mice. The left panel shows the production of IL-10 without LPS and the right panel shows production of IL-10 by macrophages stimulated with LPS. Values represent the mean±SE. *$P<0.01$; **$P<0.001$.

mouse, with the OPN-Tg mouse displaying a significantly larger fatty-streak lesion formation than the non-Tg mouse (Figure 1, upper panels). Furthermore, the thickness of the medial layer of the aorta was greater in the OPN-Tg mouse (Figure 1, middle panels). MOMA-2 staining revealed that the lesions in both mice consisted mainly of foam cells of macrophage (Figure 1, bottom panels), but more lipids were contained in the medial layer, which was not stained by MOMA-2 in the OPN-Tg mouse (Figure 1, arrow, right middle panel). After the mice were fed an atherogenic diet for 16 weeks, the aortic sinus lesions were increased in the OPN-Tg mice to a mean of 17 859±2010 μm^2 (n=12) versus the non-Tg to a mean of 6469±485 μm^2 (n=12, $P<0.001$). Analysis of the extent of atherosclerosis in the aortas en face yielded similar results with a 187% increase in the lesion aorta of OPN-Tg mice compared with non-Tg mice (0.89±0.23% and 0.31±0.01%, $P<0.001$). These results suggest that an overexpression of OPN may promote early fatty-streak lesions formation in OPN-Tg mice on an atherogenic diet.

OPN Modulation of Macrophage IL-10 Production

The recent mice studies showed that mice deficient in OPN gene expression demonstrated an increase in production of IL-10,[9] and showed that IL-10 overexpression can inhibit fatty-streak formation in the that were mice fed an atherogenic diet.[10,11] Based on the findings of these reports, we performed immunohistochemical analysis. As shown in Figure 2A, non-Tg mice expressed detectable levels of IL-10 compared with OPN-Tg mice. To clarify the contribution of

IL-10, we next examined the production of IL-10 in mice. Figure 2B shows the production of IL-10 by peritoneal macrophages from ONP-Tg and non-Tg mice. Figure 2B (left) shows the production of IL-10 without stimulation, in which both peritoneal macrophage groups released little IL-10. However, the IL-10 levels were less in the OPN-Tg mice than in the non-Tg mice (19.8±1.7 versus 34.0±2.9 pg/mL, $P<0.01$). Next, the induction of IL-10 production by LPS was performed. These results are shown in Figure 2B (right). The LPS-dependent IL-10 production of macrophages was significantly less in the OPN-Tg mice than in the non-Tg mice (81.8±7.4 versus 304.8±15.0 pg/mL, $P<0.0001$). These results show that OPN-Tg may decrease in the production of IL-10, especially under the inflammatory conditions, and a decrease of IL-10 may contribute to the susceptibility to atherosclerosis in OPN-Tg mice.

Discussion

We recently reported that there was no neointimal formation in our OPN-Tg mice fed normal chow, although OPN-Tg mice showed increased medial thickening dependent on aging. However, in the response to arterial injury, more neointima formed in OPN-Tg than in non-Tg mice.[5] These results suggest that the migration of SMCs and neointima formation by OPN are induced when the intima is impaired. Endothelial dysfunction has been reported to be induced by hypercholesterolemia.[12] As a result, we think hypercholesterolemia induced more atherosclerotic lesions in OPN-Tg than in non-Tg.

A previous study showed the expression of OPN in peritoneal cells of OPN-Tg to significantly increase,[13] and the present study demonstrated the production of IL-10 by macrophages from OPN-Tg to decrease. These results are compatible with the results of the previous study, in which OPN suppressed the LPS-dependent IL-10 response of peritoneal macrophages.[9] We think the decrease in IL-10 must contribute to the development of fatty-streak lesions. Indeed, previous studies showed that IL-10 overexpression can inhibit fatty-streak formation in mice fed an atherogenic diet,[10,11] and that IL-10 can induce endothelial cells to inhibit oxidized phospholipids-induced monocyte-endothelial interactions in vitro.[10] These reports suggested that IL-10 might inhibit atherosclerosis. Although our findings suggest that the inhibition of IL-10 in OPN-Tg may play one of the most important roles in the development of atherosclerosis, we also believe that other factors most likely play a role in this phenomenon. For example, OPN has recently been classified as a T-helper 1 cytokine because of its ability to enhance interferon-γ and IL-12 production and to diminish IL-10.[9] The strong influence toward a T-helper 1 phenotype has previously been demonstrated in an atherosclerotic model,[14,15] and therefore, we think that these factors may cause an increase of fatty-streak lesions in OPN-Tg mice. Further research is needed to clarify the mechanisms why OPN promotes atherogenesis.

Although the HDL levels decreased in the OPN-Tg, no significant difference was seen between OPN-Tg and non-Tg, and the total cholesterol levels tended to decrease in non-Tg. We thus believe that the HDL levels only slightly contributed to the increased fatty-streak lesions in OPN-Tg. The present study shows that early fatty-streak formation was promoted by OPN but the findings didn't show whether or not OPN has any effect on more mature and advanced lesions. We thus believe that the OPN overexpression must be bred onto the apoE-deficient background to determine whether or not OPN has any effect on advanced lesions. However, it remains important to determine whether OPN can be modulated by treatment, and whether or not such an approach can be used to modulate the immune responses and reduce atherosclerosis.

Acknowledgments

These studies were supported in part by New Energy and Industrial Technology Development Organization Grants.

References

1. Hirota S, Imakita M, Kohri K, et al. Expression of osteopontin messenger RNA by macrophages in atherosclerotic plaques: a possible association with calcification. *Am J Pathol.* 1993;143:1003–1008.
2. Giachelli CM, Bae N, Almeida M, et al. Osteopontin is elevated during neointima formation in rat arteries and is a novel component of human atherosclerotic plaques. *J Clin Invest.* 1993;92:1686–1696.
3. Ikeda T, Shirasawa T, Esaki Y, et al. Osteopontin mRNA is expressed by smooth muscle-derived foam cells in human atherosclerotic lesions of the aorta. *J Clin Invest.* 1993;92:2814–2820.
4. Shanahan CM, Cary NR, Metcalfe JC, et al. High expression of genes for calcification-regulating proteins in human atherosclerotic plaques. *J Clin Invest.* 1994;93:2393–2402.
5. Isoda K, Nishikawa K, Kamezawa Y, et al. Osteopontin plays an important role in the development of medial thickening and neointimal formation. *Circ Res.* 2002;91:77–82.
6. Hedrick CC, Castellani LW, Warden CH, et al. Influence of mouse apolipoprotein A-II on plasma lipoproteins in transgenic mice. *J Biol Chem.* 1993;268:20676–20682.
7. Johnson RC, Chapman SM, Dong ZM, et al. Absence of P-selectin delays fatty streak formation in mice. *J Clin Invest.* 1997;99:1037–1043.
8. Tangirala RK, Rubin EM, Palinski W. Quantitation of atherosclerosis in murine models: correlation between lesions in the aortic origin and in the entire aorta, and differences in the extent of lesions between sexes in LDL receptor-deficient and apolipoprotein E-deficient mice. *J Lipid Res.* 1995; 36:2320–2328.
9. Ashkar S, Weber GF, Panoutsakopoulou V, et al. Eta-1 (Osteopontin): an early component of type-1 (cell-mediated) immunity. *Science.* 2000;287: 860–864.
10. Mallat Z, Besnard S, Duriez M, et al. Protective role of interleukin-10 in atherosclerosis. *Circ Res.* 1999;85:e17–e24.
11. Pinderski Oslund LJ, Hedrick CC, Olvera T, et al. Interleukin-10 blocks atherosclerotic events in vitro and in vivo. *Arterioscler Thromb Vasc Biol.* 1999;19:2847–2853.
12. Busse R, Fleming I. Endothelial dysfunction in atherosclerosis. *J Vasc Res.* 1996;33:181–194.
13. Iizuka J, Katagiri Y, Tada N, et al. Introduction of an osteopontin gene confers the increase in B1 cell population and the production of anti-DNA autoantibodies. *Lab Invest.* 1998;78:1523–1533.
14. Zhou X, Paulsson G, Stemme S, et al. Hypercholesterolemia is associated with a T helper 1/Th2 switch of the autoimmune response in atherosclerotic apo E-knockout mice. *J Clin Invest.* 1998;101:1717–1725.
15. Frostegard J, Ulfgren AK, Nyberg P, et al. Cytokine expression in advanced human atherosclerotic plaques: dominance of pro-inflammatory (Th1) and macrophage-stimulating cytokines. *Atherosclerosis.* 1999;145: 33–43.

Annual Review 神経 2004

2004 年 1 月 30 日 発行

中外医学社

2. Schwartz-Jampel 症候群（軟骨異栄養性筋強直症）とパールカン

順天堂大学脳神経内科講師　平澤恵理

key words　perlecan, acetylcholinesterase, neuromuscular junction, myotonia

動　向

Schwartz-Jampel症候群（SJS）は乳幼児期に発症し，ミオトニアと骨軟骨病変を併せもつ先天性疾患である．ミオトニアの性状が筋緊張性ジストロフィーや先天性ミオトニアなどと違い，Isaacs症候群などに観察されるニューロミオトニア的要素があるとされその発症機序には異論が多い．低身長や骨格異常についてもミオトニアと一元的な症状か二次的なものかも不明であった．そのため，その病因について議論が多く，原因遺伝子の解明が期待されていた．Nicoleら[1]と著者ら[2]は臨床的にSJS1型と分類される患者において，基底膜型ヘパラン硫酸プロテオグリカンであるパールカンの遺伝子変異を同定した．これにより，臨床症状の多様性，病型の不均質性に対する分子機構の解明の大きな飛躍が期待される．これまでの文献報告例には一部パールカン遺伝子異常に起因しないものが含まれている可能性もある．今後，個々の症例の遺伝子レベル，蛋白質レベルでの解析と臨床症状の検討により，いくつかの疑問に明確な答えが示されると思われる．ここではパールカン分子とSJSの臨床症状の関連性を考察する．

A. Schwartz-Jampel症候群の臨床

1. 臨床症状

病型分類については後述するが，以下1型の臨床症状について記載する．生下時は，臨床的に異常を認めないが，次第に筋緊張亢進が明らかになり3歳位までに診断される．顔面筋の緊張のため眼裂は狭小となり，口を尖らせた仮面のような顔貌を呈する．下顎にミオキミア様の不随意収縮を認めることもある．その他の合併症として小眼症，白内障，斜視，眼振等の眼症状がある．高口蓋，低位耳介等の小奇形もしばしば合併する．精神遅滞を伴う報告もあるが一般に知能障害は認めない．本症候群は多彩な骨格異常を伴うことでも知られ，大関節の屈曲拘縮，脊椎の後彎が認められる．扁平椎体，骨端，骨幹端異形成がみられるが，骨端，骨幹端異形成は大関節に限られる．大腿骨頭の変化は比較的強く，内反股を認めることがある．低身長を認めることが多い．

2. 検査所見

筋電図所見は連続的な自発性活動電位を示し，筋の安静を保っても筋放電が終止せずに持続する．特に臨床所見の強い顔面，大腿部では筋電図所見も著明である．この自発性活動電位は低振幅

で漸減がなく長く持続するといった特徴をもつ．Taylorらは，この自発電位がクラレ curareにより減弱することから他のミオトニア症候群で観察されるミオトニア電位とは異なる可能性を示した[3]．その後も，いくつかの症例報告でSJSのミオトニアについて神経原性か筋原性かの議論が残されている．神経原性といっても神経伝導速度は正常であることから末梢神経由来ではなく，神経筋接合部の異常等も考えられる．他のミオトニア症候群に観察されるミオトニアとは違った発症機序が想定され興味深い．筋病理所見は筋線維の大小不同，中心核増生等非特異的なミオパチー様所見をとる．径の大小不同は主にタイプ1線維に認められる．神経原性所見は一般に観察されない．興味深い所見としては，アセチルコリンエステレース（AChE）染色が神経筋接合部に局在せず，大径の線維を中心に筋表面膜全体に認めるという特異的な所見を認めた症例報告がある[4]．電子顕微鏡的所見としては，筋形質拡大，筋原線維束間の空胞，筋原線維およびZ板の断裂等が認められ，神経終板には大きな変化がなかったという報告がある．クレアチンカイネース（CK）値は正常あるいは，経過とともに軽度上昇する．

3. 臨床病型分類と連鎖解析

SJSの遺伝形式は，常染色体劣性遺伝様式をとるとされるが常染色体優性遺伝型を示した家系の報告もある[5]．1962年にSchwartzらによって“Congenital blepharophimosis associated with a unique generalized myopathy”として報告されて以後，50例以上が文献的に報告されてきたが，臨床症状，発症様式の多様性を認め，その病因も不明であった．臨床的に出生時には明らかな異常を認めず，成長とともにミオトニアと骨格系の異常が出現するものを1A型，出生後まもなくから骨格の異常が明らかになるものを1B型とされる．さらに出生時より骨格異常が強く予後の悪い重症型が新生児型，あるいは2型と分類されるが，連鎖解析の結果2型は染色体1番に連鎖しないことから，遺伝的病因は均一ではないと考えられている[6]．現在のところSJS2型は神経筋疾患と骨軟骨異常を合併し，乳児期致死を呈するStuve-Wiedemann症候群と同一の疾患ととらえる方向にある[7]．Schwartzらの原著症例は1型と考えられるが1歳時から症状が出現しており，1A型と1B型の分類は必ずしも容易ではないと思われる．我々が遺伝子検索した3症例のうち，最も軽症と考えられた症例1は骨格異常も比較的軽く1A型と考えられる[8]．NicoleらはSJS遺伝子座を染色体1番1p36.1-1p34に局在することを示し[9]，さらにこの領域をせばめることにより，1p36.1-p35にマップされていたパールカン遺伝子（perlecan: *HSPG2*）がSJS遺伝子座に含まれることをみいだした．さらに3家系のSJSでエクソンスキッピング，ミスセンス，ノンセンス変異の3種類のhomozygous mutationを報告した[1]．我々もこれとは独立に3症例5種類のパールカン遺伝子変異を報告した[2]．

B. SJSの原因遺伝子パールカンの分子生物学

SJSの原因遺伝子としてミオトニアや骨病変の発症のメカニズムとの関連性に興味がもたれているパールカンであるが，本来基底膜の主要構成成分として同定されたヘパラン硫酸プロテオグリカンで，多様な生物学的活性をもつ多機能細胞外マトリックスとして知られている．パールカンはラミニン，ナイドジェン，フィブロネクチン，IV型コラーゲン等の細胞外マトリックスと結合して基底膜を構成する構造蛋白質である一方，FGFをはじめとする成長因子やその細胞膜受容体とも結合して様々な細胞内シグナルを修飾，制御する機能分子としても働き，器官の形態形成過程にお

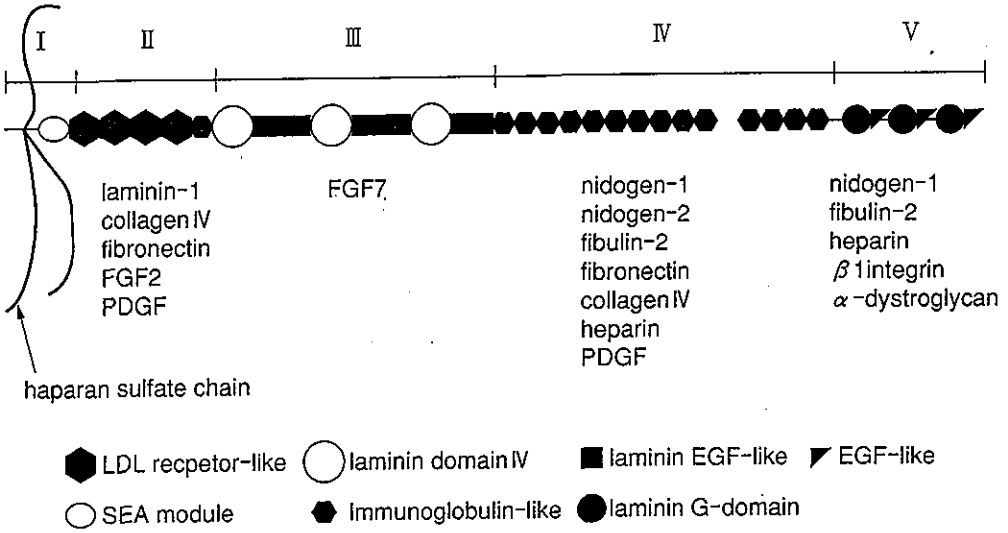

図1 パールカン分子の機能ドメインとその結合蛋白質（文献11より一部改変）
ドメインI: 3カ所のヘパラン硫酸鎖の結合部位が存在する．ドメインII: LDL受容体のLDL結合部位の配列と相同性があり，4つのシステインに富むモチーフが存在する．ドメインIII: ラミニンの短鎖のN末端領域と高い相同性をもち，3つの球状のサブドメインとEGF様の繰り返し配列をもつ．ドメインIV: この領域の前半は他の基底膜蛋白質と結合性をもち，パールカンの細胞外マトリックスでの局在に重要である．ドメインV: ラミニンα鎖のC末端球状Gドメインと相同性をもつ球状サブドメインと，EGF様繰り返し配列からなり，α-ジストログリカンやインテグリンβ1との強い結合性から細胞接着等の機能が想定される．

ける上皮-間充織相互作用に重要であるとされている．また，血管新生，組織の修復，癌細胞の増殖，転移，浸潤等に関与していると考えられている．コア蛋白質は400kDa以上あり，5つの機能ドメインをもち，各ドメインの生物学的活性は*in vitro*の研究成果から図1のように報告されている[10]．

C. マウスおよびヒトにおけるパールカン遺伝子の変異と病態

1. パールカンノックアウトマウスの作成とその表現型

我々はこの多様な機能をもつパールカンの*in vivo*での役割を明らかにし，その欠損が発生にどのような障害をもたらすか，また，どのような疾患を引き起こすのかを調べるため，パールカン遺伝子のノックアウトマウスを作成した．このマウスの一部は頭部形成異常のため胎生10.5日頃に早期胎生期致死を呈するが，大部分のものは軟骨異形成症による周産期致死を呈することがわかった[12]．ほぼ同時期にCostellらの作成したマウスからも同様の表現型が報告された[13]．変異マウスは，内軟骨性骨化の障害により明らかな四肢短縮を呈するが，膜性骨化は障害されないため，四肢長管骨は横径が増し，太く短く発達する．脊椎の椎体部分の発生も内軟骨性骨化によるので，長管骨と同様の変化をとる．また胎生後期まで生存し，軟骨形成異常を呈したマウスの一部で脳ヘルニアも合併した．

2. パールカン機能完全欠損による遺伝性疾患の同定と遺伝子解析

ノックアウトマウスの解析結果から，これまで考えられてきた基底膜の主要構成成分としての役割のみならず，軟骨発生分化におけるパールカンの重要性が示された．基底膜をもたない軟骨組織において，致命的な形成異常を示したことは予想

外の結果であったが，その後ヒトでのパールカン欠損病をみいだす大きな鍵を与えた．我々は，パールカン欠損マウスの表現型から，ヒトでのパールカン欠損疾患が存在するものと考え，その探索を開始した．候補となる疾患の同定に際しては，ヒトでのパールカン欠損病でもノックアウトマウスと同じような表現型を呈する可能性から，ノックアウトマウスでの特徴的な骨X線所見，骨成長板の異常病理所見と合致する常染色体劣性遺伝形式軟骨異形成症を捜した．その結果，周産期致死性の軟骨異形成症（Silverman-Handmaker型 dyssegmental dysplasia: DDSH）の表現型がパールカンノックアウトマウスのそれと大変類似していることがわかった[14]．この疾患では患児は体幹，四肢とも著しく短縮し，四肢長管骨の彎曲，椎体骨の大小不同等ノックアウトマウスと非常によく似た骨格異常を示すが，さらに一部の例で，脳ヘルニアを合併するとされる点もノックアウトマウスと共通し，非常に有力な候補と考えられた．この遺伝子は100kb以上の巨大遺伝子であるためその欠損病を捜すアプローチとして，1．各ドメインに対する抗体を用いた免疫染色によりスクリーニングを行い，2．cDNAを用いたRT-PCRでmRNAレベルの異常を検出し，3．染色体DNAレベルでの変異を同定するというアプローチを用いて，パールカン遺伝子変異を探索した．その結果3症例2種類の遺伝子変異を同定した．これらの変異は，おのおのフレームシフトを起こし変異の直後で転写を終了するアウトオブフレーム変異であった．我々はさらに，蛋白質レベルの解析を行い，遺伝子変異によりこの疾患ではパールカンが細胞外に分泌されず，細胞外マトリックスとして機能しないことがわかった．すなわち，パールカン機能完全欠損に起因する疾患と考えられた．

3. パールカン機能部分欠損による遺伝性疾患: SJSの同定と遺伝子解析

ところで，パールカン分子は，前述したように，複数のドメインからなる巨大な多機能分子であり，部分欠損などによるその他の表現型も考慮する必要がある．そこで，我々はパールカン遺伝子がマップされている染色体1p36に連鎖する疾患を探したところ，SJSが候補としてあげられた．詳細なマッピングを行ったところ，SJSの遺伝子座が，パールカン遺伝子座と450kb以内の距離にあることがわかった．SJSは，ミオトニア症状と軟骨異常を伴う遺伝性疾患でDDSHと異なり患者は生存する．骨格異常を伴うことから，パールカン異常による疾患である可能性が強く示唆された．また，ミオトニア症状に関しても，以下の理由からパールカン異常と関連する可能性が考えられた．パールカンは筋細胞をとりまく基底膜に局在し，特に神経筋結合部（NMJ）には多く存在する（図2）．パールカン分子の生物学的機能の一つに，NMJ特異的な非対称型AChEのコラーゲン様ドメイン collagen-like tail（ColQ）と結合

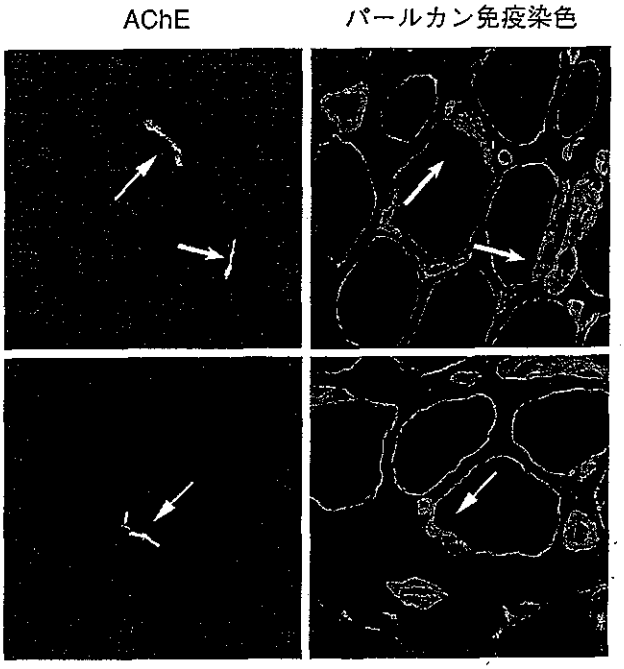

図2　神経筋接合部におけるパールカンとAChEの共局在

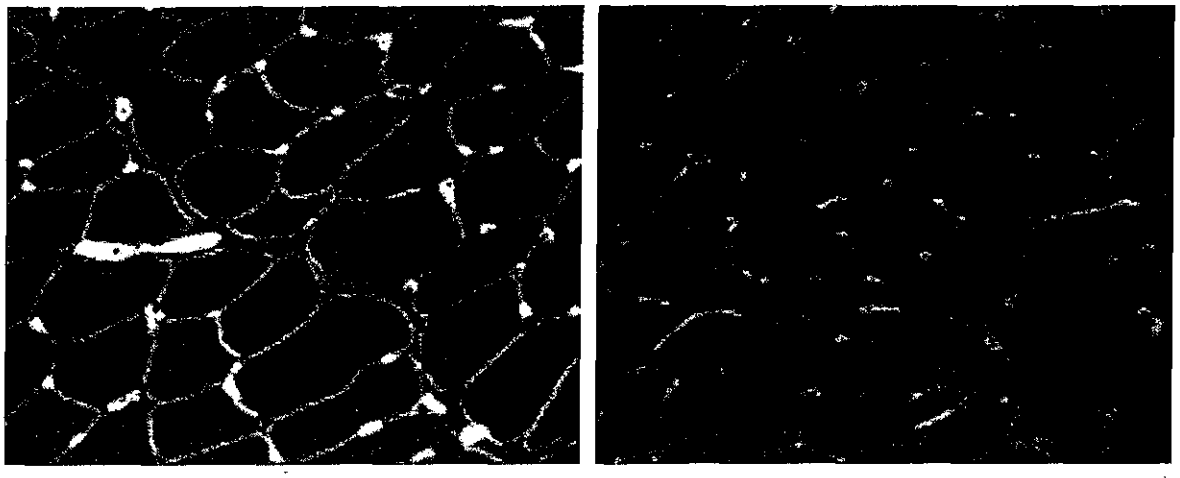

コントロール　　SJS

図3　生検筋のパールカン免疫染色（文献2より改変）

することが知られている[15]．ColQはAChEの構造のうち神経筋接合部基底膜に接着する尾部構造である[16]．それゆえ，パールカンは神経筋接合部（NMJ）の基底膜にAChEを結合，集束させることにより，アセチルコリン（ACh）による神経筋の興奮とその解除を速やかに調整していると考えられ，その欠損は筋の収縮活動に異常をきたす可能性が充分考えられる．このように，遺伝子座の一致と臨床症状の特徴からSJSをパールカン異常による第二の疾患の有力な候補と考え，前述のアプローチを進め，前述のように遺伝子変異を確認した．さらに我々は，SJSでの蛋白質レベルの解析を行い，DDSHと違いSJSではパールカンが細胞外に分泌され，筋基底膜に局在しているということを確認した（図3）．すなわち，パールカン機能部分欠損による遺伝性疾患として同定した．これはDDSHがSJSと比べ，明らかに良好な経過をとる大きな理由と考えられた．

D．先天性筋無力症候群とSJSにおけるAChE欠損と発症機構

先にSJSにおけるパールカン分子の欠損が，AChEの神経筋接合部（NMJ）基底膜への結合，集束に影響し，神経筋の興奮とその解除に異常をきたす可能性について述べた．パールカン遺伝子異常が確認されているSJS患者生検筋に神経筋接合部が含まれていない場合，生検標本においてこれを確認することは困難である．我々は，パールカンノックアウトマウスにおける神経筋接合部の解析を行った．機能完全欠損であるノックアウトマウスは出生時までに死亡するが，神経筋接合部発生，形成を観察することができる．新生ノックアウトマウスの横隔膜，肋間筋，骨格筋等において末梢神経の支配，神経筋接合部へのアセチルコリン受容体，アグリン，ラプシン等の分子の集合などがみられほぼ正常な神経筋接合部が形成されているにもかかわらずAChEの局在のみが欠損していることを示した[17]．筋全体の生化学的検討ではAChEの各アイソフォームは確認されたことから，生成されたAChEの基底膜への局在化の障害と考えられた．終板AChEの欠損する疾患として先天性終板AChE欠損症がある[18,19]．これは常染色体劣性のまれな疾患で，ColQ遺伝子の異常により終板におけるAChEの欠損を引き起こす．臨床的には乳児期または小児期に始まる易疲労性と脱力を主症状とする先天性筋無力症候群で，躯幹筋の脱力と易疲労性のため，起立歩行

時に側彎，前彎などの姿勢異常を示す．AChEの欠損症ではシナプス間隙に過剰のAChが存在する．このため，AChRの開口時間の延長による脱分極性ブロックやAChRの脱感作をきたし，神経筋伝達が阻害され筋力低下の原因となる[18-20]．脱分極の程度が軽い場合はブロックではなく持続性の筋収縮をきたす可能性があり，SJSにおけるミオトニア発生機序として想定される．最近筆者らは，パールカンノックアウトマウスの軟骨異常をレスキューすることにより延命をはかり，パールカンの欠損による筋，神経筋接合部の変化を形態的，生理学的幅広く解析することを試みており，これによりSJSの発症機序の解明がさらに進むことが期待される．先天性終板AChE欠損症とSJSはともにAChEの欠損を示す病態としてその異同は非常に興味深く，今後の研究発展がのぞまれるところである．

現在のところSJSに対する治療は対症療法にとどまるが，今後，蛋白質レベルでの異常と臨床症状の関連性等の解明により，発症のメカニズムが明らかになり，症状の軽減特にミオトニアのコントロールが効率的に行えることが望まれる．

文献

1) Nicole S, Davoine CS, Topaloglu H, et al. Perlecan, the major proteoglycan of basement membranes, is altered in patients with Schwartz-Jampel syndrome(chondrodystrophic myotonia). Nat Genet 2000; 26: 480-3.
2) Arikawa-Hirasawa E, Le AH, Nishino I, et al. Structural and functional mutations of the perlecan gene cause Schwartz-Jampel syndrome, with myotonic myopathy and chondrodysplasia. Am J Hum Genet 2002; 70: 1368-75.
3) Taylor RG, Layzer RB, Davis HS, et al. Continuous muscle fiber activity in the Schwartz-Jampel syndrome. Electroencephalogr Clin Neurophysiol 1972; 33: 497-509.
4) Fowler WM Jr, Layzer RB, Taylor RG, et al. The Schwartz-Jampel syndrome. Its clinical, physiological and histological expressions. J Neurol Sci 1974; 22: 127: 46.
5) Pascuzzi RM, Gratianne R, Azzarelli B, et al. Schwartz-Jampel syndrome with dominant inheritance. Muscle Nerve 1990; 13: 1152-63.
6) Brown KA, al-Gazali LI, Moynihan LM, et al. Genetic heterogeneity in Schwartz-Jampel syndrome: two families with neonatal Schwartz-Jampel syndrome do not map to human chromosome 1p34-p36.1. J Med Genet 1997; 34: 685-7.
7) Cormier-Daire V, Superti-Furga A, Munnich A, et al. Clinical homogeneity of the Stuve-Wiedemann syndrome and overlap with the Schwartz-Jampel syndrome type 2. Am J Med Genet 1998; 78: 146-9.
8) Ho NC, Sandusky S, Madike V, et al. Clinico-pathogenetic findings and management of chondrodystrophic myotonia (Schwartz-Jampel syndrome): a case report. BMC Neurol 2003; 3: 3.
9) Nicole S, Ben Hamida C, Beighton P, et al. Localization of the Schwartz-Jampel syndrome (SJS) locus to chromosome 1p34-p36.1 by homozygosity mapping. Hum Mol Genet 1995; 4: 1633-6.
10) Iozzo RV. Perlecan: a gem of a proteoglycan. Matrix Biol 1994; 14: 203-8.
11) Arikawa-Hirasawa E, Yamada Y. [Roles of perlecan in development and disease: studies in knockout mice and human disorders]. Seikagaku 2001; 73: 1257-61.
12) Arikawa-Hirasawa E, Watanabe H, Takami H, et al. Perlecan is essential for cartilage and cephalic development. Nat Genet 1999; 23: 354-8.
13) Costell M, Gustafsson E, Aszodi A, et al. Perlecan maintains the integrity of cartilage and some basement membranes. J Cell Biol 1999; 147: 1109-22.
14) Arikawa-Hirasawa E, Wilcox WR, Le AH, et al. Dyssegmental dysplasia, Silverman-Handmaker type, is caused by functional null mutations of perlecan. Nat Genet 2001; 23: 354-8.
15) Steen MS, Froehner SC, PerleCan fix your muscle AChEs. Trends Neurosci 2003; 26: 241-2.
16) Krejci E, Thomine S, Boschetti N, et al. The mammalian gene of acetylcholinesterase-associated collagen. J Biol Chem 1997; 272: 22840-7.
17) Arikawa-Hirasawa ERS, Rotundo RL, Yamada Y. Absence of acetylcholinesterase at the neuromuscular junctions of perlecan-null mice. Nat Neurosci 2002; 5: 119-23.
18) Engel AG, Ohno K, Sine SM, Congenital myasthenic

syndromes: progress over the past decade. Muscle Nerve 2003; 27: 4-25.
19) 福留隆泰.〔神経筋接合部疾患の病態へのアプローチ〕先天性筋無力症候群の診断と病態へのアプローチ. 臨床脳波(0485-1447)2002; (44) 9: 562-5.
20) Kohara N, Lin TS, Fukudome T, et al. Pathophysiology of weakness in a patient with congenital endplate acetylcholinesterase deficiency. Muscle Nerve 2002; 25: 585-92.

THE JOURNAL OF BIOLOGICAL CHEMISTRY
Vol. 279, No. 11, Issue of March 12, pp. 10286–10292, 2004
Printed in U.S.A.

Laminin α2 Is Essential for Odontoblast Differentiation Regulating Dentin Sialoprotein Expression*

Received for publication, September 9, 2003, and in revised form, December 1, 2003
Published, JBC Papers in Press, December 16, 2003, DOI 10.1074/jbc.M310013200

Kenji Yuasa‡§¶, Satoshi Fukumoto‡¶‖, Yoko Kamasaki‡, Aya Yamada‡, Emiko Fukumoto, Kazuhiro Kanaoka§, Kan Saito‡, Hidemitsu Harada‡‡, Eri Arikawa-Hirasawa§§, Yuko Miyagoe-Suzuki¶¶, Shinichi Takeda¶¶, Kuniaki Okamoto§, Yuzo Kato§, and Taku Fujiwara‡**

*From the ‡Division of Pediatric Dentistry and §Oral Molecular Pharmacology, Department of Developmental and Reconstructive Medicine, and **Division of Oral Health Services Research, Department of Public Health, Nagasaki University Graduate School of Biomedical Sciences, 1-7-1 Sakamoto, Nagasaki 852-8588, ‡‡Department of Oral Anatomy and Developmental Biology, Osaka University Graduate School of Dentistry, 1-8 Yamadaoka, Suita, Osaka 565-0871, the §§Department of Neurology, Juntendo University School of Medicine, 2-1-1 Hongo, Bunkyo-ku, 113-8421 Tokyo, and the ¶¶Department of Molecular Therapy, National Institute of Neuroscience, National Center of Neurology and Psychiatry, 4-1-1 Ogawa-higashi, Kodaira, Tokyo 187-8502, Japan*

Laminin α2 is subunit of laminin-2 (α2β1γ1), which is a major component of the muscle basement membrane. Although the laminin α2 chain is expressed in the early stage of dental mesenchyme development and localized in the tooth germ basement membrane, its expression pattern in the late stage of tooth germ development and molecular roles are not clearly understood. We analyzed the role of laminin α2 in tooth development by using targeted mice with a disrupted *lama2* gene. Laminin α2 is expressed in dental mesenchymal cells, especially in odontoblasts and during the maturation stage of ameloblasts, but not in the pre-secretory or secretory stages of ameloblasts. *Lama2* mutant mice have thin dentin and a widely opened dentinal tube, as compared with wild-type and heterozygote mice, which is similar to the phenotype of dentinogenesis imperfecta. During dentin formation, the expression of dentin sialoprotein, a marker of odontoblast differentiation, was found to be decreased in odontoblasts from mutant mice. Furthermore, in primary cultures of dental mesenchymal cells, dentin matrix protein, and dentin sialophosphoprotein, mRNA expression was increased in laminin-2 coated dishes but not in those coated with other matrices, fibronectin, or type I collagen. Our results suggest that laminin α2 is essential for odontoblast differentiation and regulates the expression of dentin matrix proteins.

Tooth development is regulated by sequential and reciprocal interactions between neural crest-derived mesenchymal cells and the oral environment (1–3); however, the precise molecular mechanisms mediating interactions between epithelium and mesenchymal cells are not clear, although basement membrane (BM)[1] components have been shown to play important roles in these regulatory events. In addition, the extracellular matrix layer, whose main components are laminin, collagen IV, nidogen, and sulfated proteoglycan, and the BM layer are both considered to be involved with cell proliferation and differentiation (4, 5).

The laminin family is composed of BM proteins that have been implicated in diverse functions of epithelial and mesenchymal cells. Each member is a heterotrimer composed of α, β, and γ chains, and five α, three β, and three γ chains have been identified and are known to form at least 15 heterotrimer structures. Most laminin family members have been found to have combinations of β1γ1 or β2γ1 chains with one of the five α chains, although laminin-5 has a unique chain composition, α3β3γ2.

Laminin-2 (with α2, β1, and γ1 chains), also known as merosin, is a major component of BM proteins in skeletal muscle and the peripheral nervous system (6), and the absence of the laminin α2 chain causes merosin-deficient congenital muscular dystrophy (MD-CMD) (7), which characteristically involves skeletal muscle along with the peripheral and central nervous systems (8). MD-CMD causes degradation, regeneration, interstitial fibrosis, and adipose tissue infiltration in skeletal muscle. Dystrophic (dy/dy) mice also display a severe reduction in laminin α2 chain expression and are accepted as an animal model of MD-CMD (6, 9–11). We generated a null mutant lacking the laminin α2 chain using a gene-targeting technique to examine the molecular pathophysiology of MD-CMD (12). The mice showed symptoms similar to those seen in MD-CMD and a shorter life span than dy/dy mice (13).

During tooth development, the mRNA of three laminin α chains, α1, α2, and α4, is expressed in tooth mesenchymal cells, whereas two other types, laminin α3 and α5 chain mRNA, are found in epithelial cells (14, 15). Furthermore, laminin α5 mRNA is widely expressed in tooth epithelium, with the corresponding protein distributed along the tooth basement membrane during the embryonic stage and diminished at the start of enamel matrix production (14). Laminin α3 expression is slight in the embryonic stage and then dramatically increases during terminal differentiation of ameloblasts, following degradation of the tooth BM (14, 16). On the other hand, laminin

* This work was supported by Grants-in-aid for Scientific Research in a Priority Area 15689025 and 15791255 from the Ministry of Education, Science, Sports and Culture of Japan. The costs of publication of this article were defrayed in part by the payment of page charges. This article must therefore be hereby marked "*advertisement*" in accordance with 18 U.S.C. Section 1734 solely to indicate this fact.

¶ Both authors contributed equally to this work.

‖ To whom correspondence should be addressed: Division of Pediatric Dentistry, Dept. of Developmental and Reconstructive Medicine, Nagasaki University Graduate School of Biomedical Sciences, 1-7-1 Sakamoto, Nagasaki 852-8588, Japan. Tel.: 81-95-849-7674; Fax: 81-95-849-7675; E-mail: satoshi@dh.nagasaki-u.ac.jp.

[1] The abbreviations used are: BM, basement membrane; DSP, dentin sialoprotein; DMP, dentin matrix protein; MD-CMD, merosin-deficient congenital muscular dystrophy; DSPP, dentin sialophosphoprotein; AMBN, ameloblastin; AMEL, amelogenin; PBS, phosphate-buffered saline; RT, reverse transcription/transcriptase; G3PDH, glyceraldehydes-3-phosphate dehydrogenase; AI, amelogenesis imperfecta; ANOVA, analysis of variance; SEM, scanning electron microscope; LG, laminin-type G.

α2 mRNA is detected in mesenchymal cells in the tooth germ. In the earlier stages, mesenchymal expression is seen around the epithelial bud, while in later stages (E15–18) laminin α2 mRNA expression becomes stronger in dental sac cells than in dental papilla cells. By using immunohistostaining, laminin α2 can be detected in the tooth germ BM before E15, although later (E15–18) staining is lost from the dental BM, the area between the inner dental epithelium and dental papilla mesenchyme layers, whereas it remains strong in the BM area between the outer dental epithelium and dental sac mesenchyme (14). However, the expression and molecular mechanisms of laminin α2 in postnatal tooth development have not been clearly shown.

In the present study, we examined tooth formation and dentin sialoprotein (DSP) expression in laminin α2 knockout mice, a mutant strain with thin enamel and a widely opened dentinal tube, which are caused by a reduction of dentin formation and odontoblast differentiation. Laminin-2 enhances the expression of dentin sialophosphoprotein (DSPP) and dentin matrix protein (DMP) in primary cultured dental mesenchymal cells. Our present findings suggest that interactions between laminin α2 and odontoblasts regulate their differentiation and are important for dentinogenesis.

EXPERIMENTAL PROCEDURES

Scanning Electron Microscope (SEM) Analysis—Incisors were taken from wild-type and laminin α2 null mice and coated with gold and photographed using scanning electron microscopy at 20 kV (S-3500, Hitachi Ltd., Tokyo, Japan). To observe the enamel crystals and dentinal tubes, the specimens were embedded in epoxy resin, cut with an ISOMET low speed saw (Buehler, Lake Bluff, IL), and then treated with 40% phosphoric acid for 10 s and 10% sodium hypochlorite for 30 s, prior to coating with gold.

Preparation of Tissue Sections—Laminin α2 null mice were generated by gene targeting and housed in a pathogen-free animal facility. Standard Nagasaki University guidelines were followed to monitor their health status as well as the housing and breeding practices. To prepare the heads of 3-week-old mice, each animal was anesthetized and then fixed by perfusion with 4% paraformaldehyde/PBS. The maxilla was dissected out, post-fixed overnight at 4 °C in 4% paraformaldehyde/PBS, and decalcified with 250 mM EDTA/PBS for 2 weeks, then dehydrated in xylene through a graded ethanol series, and embedded in paraplastic paraffin (Oxford Laboratories). Sections were cut at 10 μm on a microtome (RM2155, LEICA, Inc.). For detailed morphological analyses of molars and incisors, sections were stained with Harris hematoxylin and eosin Y (Sigma). For staining of cultured cells, cells were fixed with 4% paraformaldehyde, 0.5% Triton X-100, PBS for 5 min and then 4% paraformaldehyde/PBS for 10 min.

Immunohistochemistry—Immunohistochemistry was performed on the sections, which were incubated in 1% bovine serum albumin/PBS as a blocking agent for 1 h prior to incubation with primary antibodies. We used antibodies directed against laminin α2 (4H8–2, Alexis) (12), ameloblastin (AMBN) (17), amelogenin (AMEL) (18, 19), and DSP (20) (provided by Yoshihiko Yamada). The primary antibodies were detected using fluorescein isothiocyanate or Cy-3-conjugated secondary antibodies (Jackson ImmunoResearch).

Dental Epithelial and Mesenchymal Cell Cultures—For dental mesenchymal cell cultures, P3 mouse molars were dissected and treated with 0.1% collagenase, 0.05% trypsin, 0.5 mM EDTA for 10 min, after which the dental mesenchyme was separated from the dental epithelium. Separated dental mesenchyme samples were treated with 0.1% collagenase, 0.05% trypsin, 0.5 mM EDTA for 15 min and then collected using a pipette and placed into the wells (21). Dental mesenchymal cells were cultured in Dulbecco's modified Eagle's medium (Invitrogen) with 10% fetal calf serum, whereas a dental epithelial cell line (HAT-7) was cultured in Dulbecco's modified Eagle's medium/F-12 with 10% fetal calf serum (22).

RNA Isolation and RT-PCR—Developing molars were dissected from P3 mice, and RNA was isolated using TRIzol reagent, according to the manufacturer's instructions (Invitrogen). First strand cDNA was synthesized at 42 °C for 90 min using oligo(dT)$_{14}$ primer. Real time PCR amplification was performed using primers for AMBN (5′-GCGTTTCCAAGAGCCCTGATAAC-3′ and 5′-AAGAAGCAGTGTCACATTTCCTGG-3′), AMEL (5′-ATTCCACCCCAGTCTCATCAG-3′ and 5′-CCACTTCGGTTCTCTCATTTTCTG-3′), enamelin (5′-GTGAGGAAAAATACTCCATATTCTGG-3′ and 5′-GTTGAAGCGATCCCTAAGCCTGAAGCAG-3′), enamelysin (MMP-20) (5′-AGATGGTGGCAAGAGAA-3′ and 5′-GAGATTCCGTATGTCAAAAT-3′), DSPP (5′-CTCAGAGAGAATCTGGGTGTACCACC-3′ and 5′-CACAGTGGTACATGGAGAGCTC-3′), DMP (5′-GCTTCAGGCTCAGTCTTGCT-3′ and 5′-TGTAACCCTCCAACTCCAGG-3′), osteonectin (5′-GTCTCACTGGCTGTGTTGGA-3′ and 5′-AAGACTTGCCATGTGGGTTC-3′), osteopontin (5′-CGATGATGATGACGATGGAG-3′ and 5′-GAGGTCCTCATCTGTGGCAT-3′), osteocalcin (5′-CCTCTTGAAAGAGTGGGCTG-3′ and 5′-CCTCGGGAGACAAACAACAT-3′), and G3PDH (5′-CCATCACCATCTTCCAGGAG-3′ and 5′-GCATGGACTGTGGTCATGAG-3′), with SYBR Green PCR Master Mix by TaqMan 7700 Sequencer Detection (Applied Biosystems). PCR was performed for 40 cycles, 95 °C for 1 min, 58 °C for 1 min, and 72 °C for 1 min as reported previously (21).

Cell Proliferation and Cell Binding—Dental epithelial cells (HAT-7) and dental mesenchymal cells at 1.0×10^5 were cultured in a 60-mm diameter dish coated with or without laminin-2 (merosin, Invitrogen), type I collagen (Cellmatrix, NITTA GERATIN, Japan), and fibronectin (human fibronectin, Invitrogen) for 5 days. At 1, 3, and 5 days after plating, cells were treated with 0.05% trypsin, 0.5 mM EDTA, and their numbers were counted under a microscope. For cell binding, dental epithelial and mesenchymal cells were detached with 0.05% EDTA, washed with Dulbecco's modified Eagle's medium containing 0.1% bovine serum albumin, and resuspended to a concentration of 3.5×10^5/ml. Assays were performed in 96-well round-bottomed microtiter plates (Immulon-2HB, Dynex Technologies, Inc., Chantilly, VA). Wells were coated overnight at 4 °C with laminin 2, type I collagen, or fibronectin, then diluted with PBS, and blocked with 3% bovine serum albumin for 1 h at 37 °C. After washing, the cells were added to a plate and incubated for 60 min at 37 °C. Attached cells were stained for 10 min with 0.2% crystal violet (Sigma) in 20% methanol. After washing with H_2O, the cells were dissolved in 10% SDS, and absorbance at 600 nm was measured.

RESULTS

Laminin α2 Expression in Differentiated Odontoblasts and Maturation of Ameloblasts—Laminin α2 is known to be expressed in dental mesenchymal cells and localizes in the BM area between the dental epithelium and mesenchyme layers in the early stage of tooth germ development (14); however, its expression in later stages, especially in the postnatal period, has not been clearly identified. We performed immunostaining of incisor samples from 3-week-old mice to identify the localization of laminin α2, which was found expressed in the preameloblast and pre-odontoblast interfaces (Fig. 1*A*, *a*), as well as in odontoblasts, the outer side of the dental epithelium including the papillary cell layer, capillaries, and the muscle BM (Fig. 1*A*, *a* and *b*). However, laminin α2 expression was not observed in the cervical loop region or the secretory stage of ameloblasts (Fig. 1*B*, *a*). Later, in the early maturation (Fig. 1*B*, *b*) and late maturation (Fig. 1*B*, *c*) stages, laminin α2 appeared in the side of the enamel. On the other hand, laminin α2 expression was detected in odontoblasts at all stages (Fig. 1*C*). To confirm the expression in odontoblasts, immunostaining of primary cultured dental mesenchymal cells was performed, and laminin α2-positive cells were found expressed in DSP (Fig. 1*D*), which is a marker of odontoblasts, indicating that the odontoblasts produced laminin α2.

Decreased Dentin Formation and Amelogenesis Imperfecta in Laminin α2 Null Mice—For the targeted disruption of LAMA2, a PGK-neo gene was inserted into the laminin α2 chain (12). These mice had been back-crossed into the BALB/c strain at least 10 times, before the tooth phenotype was analyzed. To examine laminin α2 expression in the masseter muscle, we performed immunostaining of 3-week-old wild-type, heterozygous, and null mutant mice, using rat anti-laminin α2 chain monoclonal antibody 4H8–2, which recognizes the 300-kDa portion of the protein (23). The results confirmed the absence of the laminin α2 chain in mutant strain muscles. Laminin α2-positive staining was observed in the muscle BM (Fig. 2*A*, *a* and *b*) in the wild-type and heterozygote mice but not in the

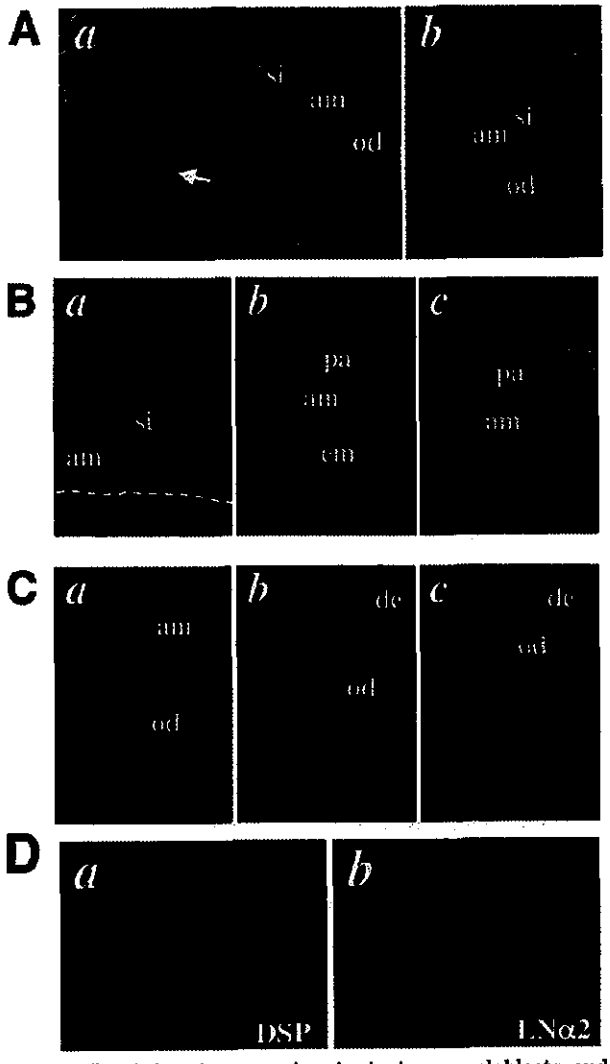

FIG. 1. **Laminin α2 expression in incisor ameloblasts and odontoblasts.** *A*, 3-week-old mice incisor cells were immunostained with anti-laminin α2 antibody as described under "Experimental Procedures." *a*, laminin α2 expression was found in the pre-ameloblast and odontoblast interface (*arrow*), and it continued in the secretory stage (*b*). *B*, higher magnification of incisor ameloblasts in each stage. Laminin α2 expression was not observed in secretory stage ameloblasts (*a*). Later, in the early maturation (*b*) and late maturation (*c*) stages, laminin α2 appeared in the side of the enamel. It was also detected in the outer side of the dental epithelium as well as the papillary cell layer in all stages. *C*, higher magnification of incisor odontoblasts in each stage corresponding to the ameloblast developmental stages as shown in *B*. Laminin α2 expression was detected in odontoblasts at all stages (*a–c*). *D*, primary cultured dental epithelial cells were stained with anti-DSP (*a*) and laminin α2 (*b*) antibodies. *si*, stratum intermedium; *pa*, papillary cell layer; *am*, ameloblast; *od*, odontoblast; *em*, enamel matrix; *de*, dentin.

mutants (Fig. 2*A*, *c*). In the same mice used to analyze laminin α2 expression in the masseter muscle, the color of the incisor surface in the mutants was found to be white when compared with the wild-type and heterozygote mice, indicating amelogenesis imperfecta (AI) (Fig. 2*B*). For detailed analyses of the incisor enamel and dentin, scanning microscopic examinations were performed. The overall tooth length and shape of the upper incisors were not different between the heterozygote and mutant mice (Fig. 2*C*); however, the cross-sectional surface of the incisor was decreased, as well as the enamel and dentin thickness by ~13 and 25%, respectively, in the mutant specimens (Fig. 2, *D* and *E*). Furthermore, the surface of the superficial enamel was rough as compared with that of the heterozygote incisors, resulting in the white color (Fig. 3*d*). In contrast, the size and structure of the enamel were not different between the two types of mice. On the other hand, the dentinal tubes were opened wide in the mutant mice following treatment with phosphoric acid and sodium hypochlorite, indicating immature dentin in the surrounding area (Fig. 3*e*). In the SEM analysis, enamel surface and dentin structures were not different between the wild-type and heterozygote mice (data not shown).

Decreased Expression of DSP in Laminin α2 Null Mice—To analyze the differentiation of ameloblasts and odontoblasts in mutant mice, we performed immunohistochemistry examinations using antibodies to AMEL, AMBN, and DSP. The AMEL and AMBN expression patterns during the secretory stage of ameloblasts were not altered in mutant incisors as compared with those from the wild-type and heterozygote mice (Fig. 4*A*). Furthermore, by using hematoxylin and eosin staining of dentin and odontoblasts, the width of the predentin and shape of odontoblasts in laminin α2 null mice were shown not to be different from those of the wild-type and heterozygote mice. However, DSP expression in odontoblasts was dramatically reduced in the mutant mice teeth (Fig. 4*B*). In addition, DMP, DSPP, and osteopontin mRNA expressions in dissected incisors were also decreased in two of the mutant mice (Fig. 5), whereas DMP, DSPP, and osteopontin mRNA were highly expressed in those from the wild type. DMP mRNA expression in two mutant strains was dramatically decreased by ~60%, whereas DSP and osteopontin mRNA were decreased by ~70% (Fig. 5). These results suggest that the differentiation of odontoblasts in the mutant mice was inhibited by the absence of the laminin α2 chain.

Laminin-2 Inhibits the Expression of Enamel Matrix and Enhances Dentin Matrix Proteins—BM components in ameloblasts, including laminin and collagen IV, are known to disappear in the secretory stage and reappear in the maturation stage (14, 24, 25). In the present study, laminin α2 showed an expression pattern similar to other BM proteins (Fig. 1). To analyze the effect of laminin-2 on ameloblasts, a rat dental epithelial cell line (HAT-7) was cultured in several extracellular matrix-coated dishes for 3 days, after which marker gene expression was analyzed by RT-PCR. In HAT-7 cells, AMEL expression was inhibited by laminin 2, fibronectin, and type I collagen (Fig. 6*A*). Furthermore, enamelin and MMP-20 (enamelysin) expression was also decreased in those matrix cultures (Fig. 6*A*), whereas AMBN expression in HAT-7 was not detected under any of the tested conditions (data not shown). These results suggest that laminin-2 inhibits ameloblast differentiation in the secretory stage. Laminin α2 is known to be expressed in dental mesenchymal cells in the early stage and then transiently disappears in mesenchymal cells facing the inner dental epithelium. In the present study, this expression reappeared and continued during dentin formation. To identify the role of laminin α2 with odontoblast differentiation, dental mesenchymal cells from P3 molar tooth germ samples were cultured in laminin-2, fibronectin, and type I collagen-coated dishes, and ~15% of the cells were found to be DSP-positive by immunostaining (data not shown). Furthermore, the expression of DSPP and DMP was increased 3–4-fold in the laminin-2-coated dish, whereas there were no changes in those coated with fibronectin or type I collagen (Fig. 6*B*).

No Effect by Laminin-2 on Proliferation and Cell Binding of Dental Mesenchymal Cells—In general, the extracellular matrix is important for proliferation and differentiation of dental epithelium and mesenchymal cells. However, long term cultures of dental epithelial cells was shown to lead to an enhance-

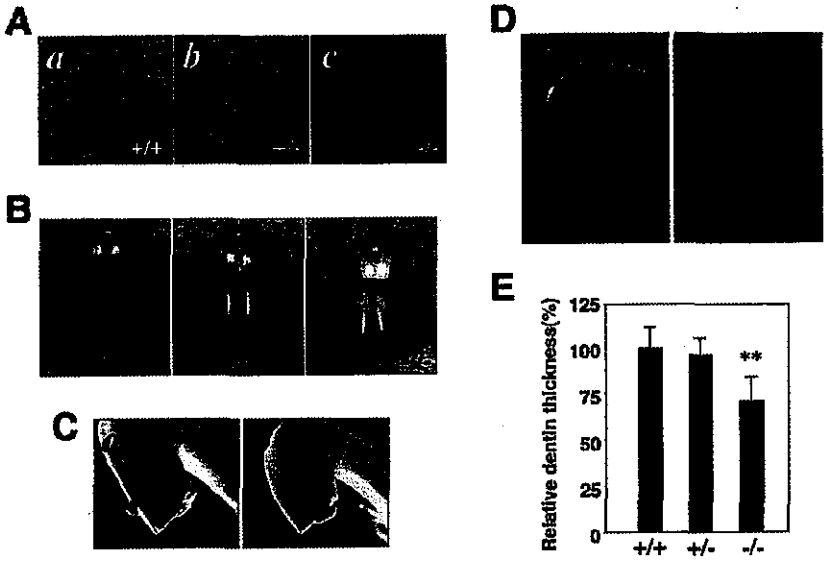

FIG. 2. **Tooth abnormalities in 3-week-old lama2−/− mice.** *A*, immunostaining with laminin α2 in masseter muscle tissues from wild-type (*a*), heterozygote (*b*), and mutant (*c*) mice. *B*, the color of the mutant incisor surfaces was white (*c*) as compared with the wild-type (*a*) and heterozygote (*b*) mice. *C*, overall tooth shape was not different between the heterozygotes (*a*) and mutants (*b*) in the SEM analysis. *D*, dentin thickness in the incisor cross-sectional surface area was decreased in the mutant (*b*) as compared with the heterozygote (*a*) mice in the SEM analysis. *E*, dentin thickness in the wild-type and heterozygote mice was not different, but dentin width in the mutants was decreased ~25%. Statistical analysis was performed using ANOVA (**, $p < 0.05$).

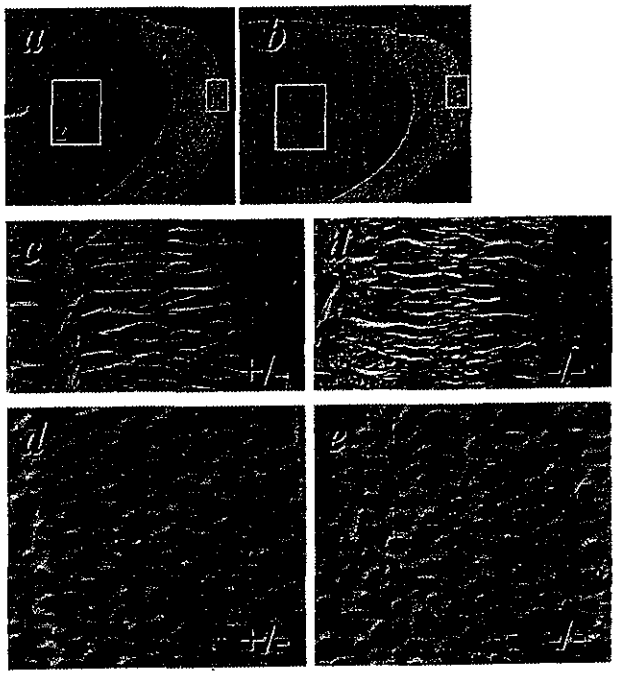

FIG. 3. **Rough surface of superficial enamel and widely opened dentinal tubes in lama2−/− mice.** SEM analysis of the incisor specimens from heterozygote (*a*, *c*, and *d*) and mutant (*b*, *d*, and *e*) mice was performed as described under "Experimental Procedures." Higher magnified images of superficial enamel (*c* and *d*) and dentinal tubes (*d* and *e*) in the *boxed region* of *a* and *b* are also shown. The superficial enamel of the mutant incisors was rough (*d*) as compared with that from the heterozygotes (*c*). The dentinal tubes were opened wide in the mutant specimens (*e*) following treatment with phosphoric acid and sodium hypochlorite.

ment of cell proliferation and decrease of the enamel matrix protein amelogenin in collagen-coated dishes (26). To determine whether the decrease of amelogenin and increase of DMP and DSPP mRNA in laminin-2-coated dishes was dependent on cell proliferation, we analyzed the effect of matrices on cell proliferation (Fig. 7). Cells were cultured with each matrix, and their numbers were counted after 5 days. HAT-7 proliferation in the type I collagen dish was increased (Fig. 7*A*), but not in the laminin-2 or fibronectin dishes, with similar results observed in the primary cultured dental mesenchymal cells (Fig. 7*B*). Type I collagen coating is known to have a greater effect on the expression of enamel matrix proteins than laminin-2 and fibronectin. Our results suggest that the decrease of enamel matrix expression in the type I collagen-coated dish may have been caused by an increase of cell proliferation. However, the decrease of amelogenin seen in dental epithelial cells and the increase of DMP and DSPP mRNA seen in dental mesenchymal cells cultured with laminin-2 may not have been dependent on cell proliferation.

Laminin is associated with several extracellular matrix and cell receptors that are important for cell binding. We hypothesized that laminin-2 directly binds to dental epithelial and mesenchymal cells and regulates the gene expression of dentin and enamel matrices. To analyze the cell binding activity of laminin-2, cells were incubated in laminin-2-coated microtiter plates as described under the "Experimental Procedures" (Fig. 8). We found that dental epithelial cell binding to laminin-2 was significantly weaker than that to fibronectin and type I collagen (Fig. 8*A*), whereas dental mesenchymal cells showed little or no binding to the laminin-2-coated plate (Fig. 8*B*).

DISCUSSION

This is the first known analysis of laminin α2 expression in differentiated ameloblasts and odontoblasts during odontogenesis and tooth development in mutant mice. Laminin α2 chain mRNA and protein are expressed in several organs besides striated muscles, including the central nervous system (6), thyroid gland, thymus, kidney, testis, skin, and digestive tract. In addition, laminin α2 is also expressed in the tooth germ during amelogenesis and dentinogenesis in a stage-specific manner (14). In the present study, laminin α2 chain mRNA was found intensely expressed in dental sac cells. Furthermore, results from immunostaining for laminin α2 expression were in conformity with the detected mRNA patterns, indicating a role for the laminin α2 chain in the production of BM proteins by dental mesenchymal cells. Salmivirta *et al.* (14) reported that no laminin α chains (α1, α2, and α4) expressed by mesenchymal cells were found in secretory odontoblasts. However, they analyzed molars from embryonic stage and postnatal day 1 mice, during which odontoblasts are partially differentiated. For this reason, we used incisors from 3-week-old mice to investigate the expression of laminin α2 chain in fully differentiated ameloblasts and odontoblasts. The BM of the cervical

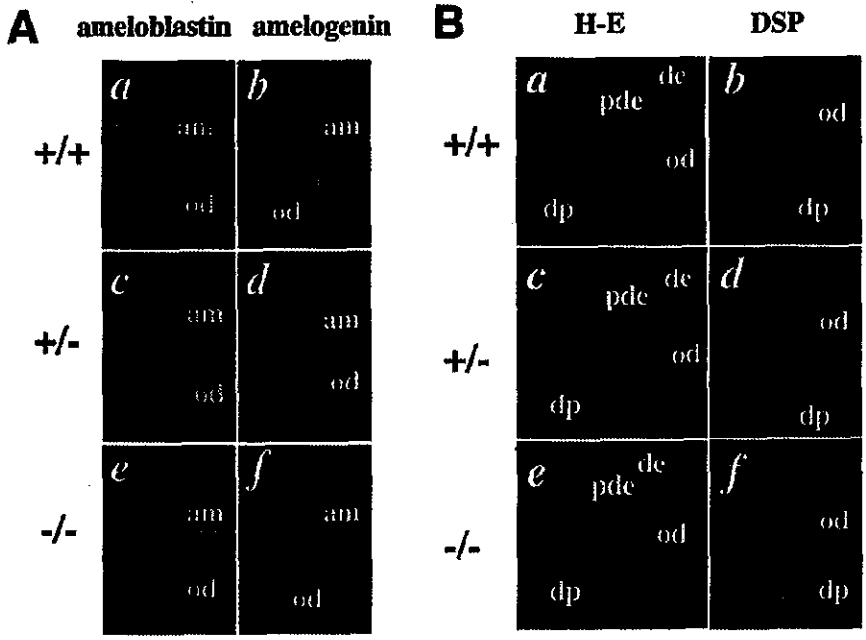

FIG. 4. **Decreased expression of DSP in lama2−/− mice.** *A*, immunostaining with anti-ameloblastin (*a*, *c*, and *e*) and amelogenin (*b*, *d*, and *f*) antibodies in secretory stage ameloblasts from wild-type (*a* and *b*), heterozygote (*c* and *d*), and mutant (*e* and *f*) mice. Ameloblastin and amelogenin expressions were not different. *B*, hematoxylin and eosin staining (*a*, *c*, and *e*) and immunostaining with anti-DSP antibody (*b*, *d*, and *f*) in differentiated odontoblasts from wild-type (*a* and *b*), heterozygote (*c* and *d*), and mutant (*e* and *f*) mice. The width of the predentin and shape of the odontoblasts in the mutants (*e*) were not different from the wild-type (*a*) or heterozygote mice (*c*). DSP expression was dramatically decreased in mutant odontoblasts (*f*). *am*, ameloblast; *od*, odontoblast; *de*, dentin; *pde*, predentin; *dp*, dental pulp.

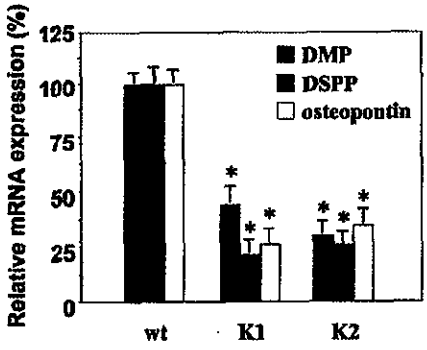

FIG. 5. **Decreased expression of DMP, DSPP, and osteopontin mRNA in lama2−/− mice.** Incisors were dissected from the maxillas of wild type (*wt*) and two mutant (K1 and K2) strains of 3-week-old mice, and then mRNA was isolated and amplified using quantitative RT-PCR, real time PCR, methods with specific primer sets as described under "Experimental Procedures." The expressions of DMP, DSPP, and osteopontin mRNA were decreased in both mutant strains. G3PDH mRNA was used as the control. G3PDH expression was not different between each sample (data not shown). mRNA expression in the mutant samples was compared with that in the wild type. Statistical analysis was performed using ANOVA (*, $p < 0.01$).

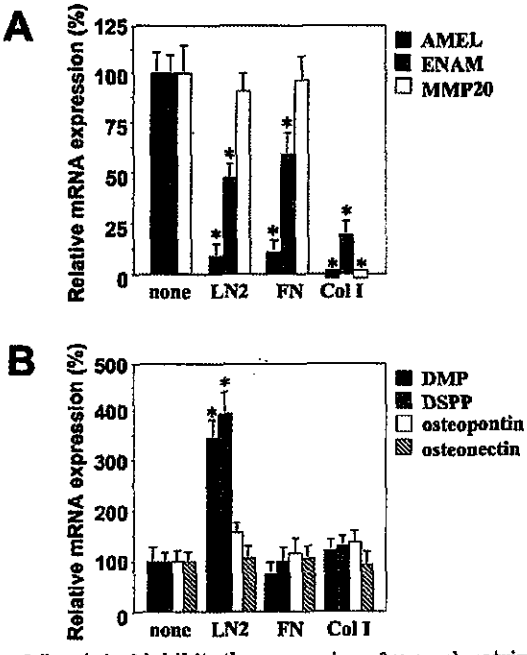

FIG. 6. **Laminin-2 inhibits the expression of enamel matrix and enhances dentin matrix proteins.** A dental epithelial cell line (HAT-7) (*A*) and primary dental mesenchymal cells (*B*) were cultured in dishes coated with or without laminin-2, fibronectin, or type I collagen for 2 days. mRNA was isolated and amplified using a quantitative RT-PCR method with specific primer sets as described under "Experimental Procedures." AMEL and enamelin (*ENAM*) expression were decreased in dental epithelial cells in laminin-2, fibronectin, and type I collagen-coated dishes. DMP and DSPP expression were increased in dental mesenchymal cells cultured in laminin-2-coated dishes. G3PDH mRNA was used as the control. G3PDH expression was not different between each sample (data not shown). These experiments were repeated at least three times with similar results. mRNA expressions in each matrix in HAT-7 and in primary cultured dental mesenchymal cells were compared with non-coated dishes. Statistical analysis was performed using ANOVA (*, $p < 0.01$).

loop in the incisor did not express the laminin α2 chain, indicating that there is no expression in inner dental epithelium or dental mesenchymal cells in molars. In contrast, expression was observed in the interface between pre-ameloblasts and odontoblasts, whereas laminin α2 transiently disappeared during odontoblast differentiation.

Because dy^{3K}/dy^{3K} mice have no laminin α2 chain, they are excellently suited for analysis of the biological functions of the laminin α2 chain in various organs (12). In the present study, we analyzed laminin α2 null mutant mice in order to identify the role of laminin α2 in the tooth development. These mice showed irregular enamel surface structures and a decrease of dentin formation, whereas ameloblasts expressed the laminin α2 chain in the maturation stage but not in the secretory stage (Fig. 1). Furthermore, enamel abnormalities were only observed in superficial enamel, because of the restriction of laminin α2 chain expression, resulting in white colored incisors. However, the structure and size of the enamel crystals were not different between heterozygote and mutant mice, because there was no laminin α2 expression in secretory stage ameloblasts.

Amelogenin and ameloblastin, tooth-specific extracellular

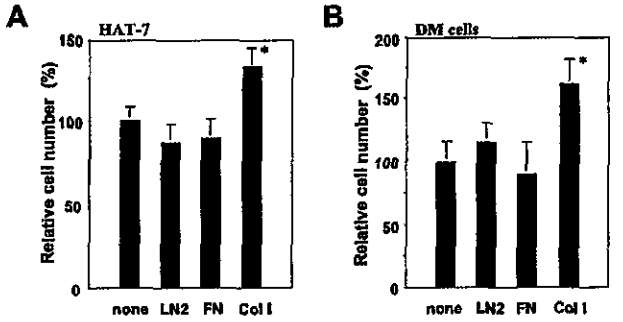

FIG. 7. **Proliferation of HAT-7 and primary dental mesenchymal cells in laminin-2, fibronectin, and type I collagen-coated dishes.** A dental epithelial cell line (HAT-7) (*A*) and primary dental mesenchymal cells (*B*) were cultured in dishes coated with or without laminin-2 (*LN2*), fibronectin (*FN*), or type I collagen (*Col I*) for 5 days. Cells were prepared and counted as described under "Experimental Procedures." Laminin-2 coating did not affect the proliferation of HAT-7 and primary dental mesenchymal cells. Type I collagen coating enhanced cell proliferation by both types of cells. These experiments were repeated at least three times with similar results. Cell proliferation in each matrix in HAT-7 and in primary cultured dental mesenchymal cells was compared with non-coated dishes. Statistical analysis was performed using ANOVA (*, $p < 0.01$).

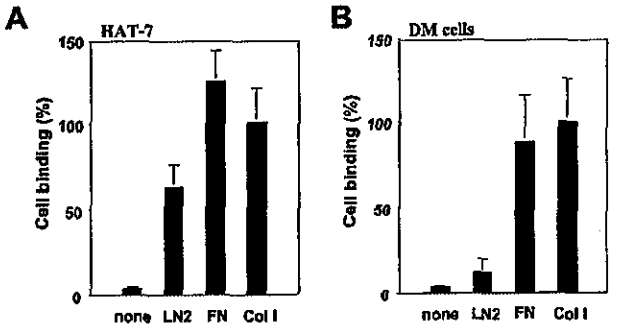

FIG. 8. **Binding of HAT-7 and primary dental mesenchymal cells to laminin-2, fibronectin, and type I collagen.** A dental epithelial cell line (HAT-7) (*A*) and primary dental mesenchymal cells (*B*) were cultured and plated on microtiter plates coated with laminin-2, fibronectin, or type I collagen. *A*, cell binding activity was analyzed as described under "Experimental Procedures." HAT-7 cells bound to laminin-2, although the binding activity was lower than to fibronectin and type I collagen. *B*, dental mesenchymal cells showed little or no binding to laminin-2-coated plates.

matrix proteins, are specifically expressed in secretory ameloblasts (17, 27–30). In patients, numerous mutations have been found in amelogenin coding sequences, with the most common genetic disorder, AI, affecting enamel (31–33). In another study, targeted disruption of the amelogenin gene locus in mice caused a hypoplastic enamel phenotype similar to AI, confirming the important role of amelogenin in enamel formation (34). Ameloblastin is also thought to have a relationship with the autosomal dominant type of AI (35). In the present laminin α2 null mutants, the expression of these enamel matrix proteins was not changed, indicating that ameloblast differentiation in the secretory stage was undisturbed, because there was no expression of laminin α2 found. Furthermore, other BM components, including collagen IV and, notably, BM proteins, were not expressed in secretory stage ameloblasts and reappeared in the maturation stage, indicating that ameloblasts may adhere to enamel surfaces via an extracellular matrix. In fact, laminin-2 was shown to have cell binding activity identical to a dental epithelial cell line, HAT-7, and did not affect cell proliferation in either HAT-7 cells or primary cultured dental mesenchymal cells.

In odontoblasts, laminin α2 expression continued during dentinogenesis. A decrease in dentin width and the occurrence of clearly opened dentinal tubes were phenotypic changes more severe than those seen in the enamel, as biomineralization of the dentin extracellular matrix requires complex interactions among several collagenous and non-collagenous molecules. Surprisingly, the expressions of Dspp mRNA and DSP protein were decreased in laminin α2 mutant odontoblasts, as Dspp was primarily found expressed by odontoblasts and pre-ameloblasts. Dspp mRNA is translated into a single protein, Dspp, and cleaved into two peptides, dentin DSP and dentin phosphoprotein (DPP), which become localized within the dentin matrix (36–40). Furthermore, the expression pattern of Dspp in odontoblasts is similar to that of laminin α2. Recently, mutations in this gene were identified in human dentinogenesis imperfecta II (Online Mendelian Inheritance in Man accession number 125490) and dentin dysplasia II (Online Mendelian Inheritance in Man accession number 125420) syndromes (41, 42). Dspp-null mice were also generated and found to develop tooth defects similar to human dentinogenesis imperfecta III with enlarged pulp chambers, an increased predentin zone width, hypomineralization, and pulp exposure (43). Interestingly, the levels of biglycan and decorin, small leucine-rich proteoglycans, were increased in the widened predentin zone and in void spaces among the calcospherites in the dentin of those null mice. Decorin also functions as an inhibitor of mineralization during primary ossification of mouse embryo bones (44), whereas biglycan facilitates the initiation of apatite formation and inhibits the growth of apatite (45). These results suggest that Dspp is essential for dentin mineralization, including the potential regulation of proteoglycan levels, and is involved in the results of the present study, as the expression of DSP and DMP was decreased in the incisors of laminin α2 null mice, indicating an inhibition of odontoblast differentiation. Similar results were observed in primary cultured dental mesenchymal cells.

It was recently reported that a lack of the laminin α2 chain results in apoptosis of myogenic cells *in vitro*, as this chain appears to promote myotube stability by preventing cell death (46). Similar results were observed in the muscle tissue cells of the present laminin α2 mutant mice, as there was a markedly high number of apoptotic nuclei that were terminal dUTP nick-end labeling-positive, as compared with wild-type littermates (12). However, in the tooth germ specimens, apoptosis was not observed in ameloblasts or odontoblasts (data not shown), and no changes in the numbers or morphology of these cells were detected. These results suggest that a reduction of dentin formation does not depend on apoptosis of dental epithelium and mesenchymal cells.

Laminin α2 did not enhance proliferation and caused no cell binding activity in the primary cultured dental mesenchymal cells; however, it did regulate the expression of dentin matrix. In contrast, type I collagen and fibronectin showed cell binding activity and enhanced the proliferation of dental mesenchymal cells. Matrix expression in primary cultured tooth germ cells was affected by cell proliferation and cell binding (26). In fact, type I collagen enhanced proliferation of both dental epithelial and mesenchymal cells and showed cell binding activity, as well as in a previous report (26). These results suggest that laminin-2 has a different function with dental mesenchymal cells, especially in contrast to odontoblasts. In addition, laminin-2 coating enhanced the expression of Dsp and Dmp, and this effect was specific to laminin-2 and corresponded to the expression of these genes in laminin α2 null mutant mice.

We also considered what kind of molecules had an interaction with laminin α2 and regulated the expression of dentin matrix proteins during dentin formation. Laminin interacts